

X-ray Sources in the Hubble Deep Field Detected by Chandra

A.E. Hornschemeier,¹ W.N. Brandt,¹ G.P. Garmire,¹ D.P. Schneider,¹ P.S. Broos,¹
L.K. Townsley,¹ M.W. Bautz,² D.N. Burrows,¹ G. Chartas,¹ E.D. Feigelson,¹ R. Griffiths,³
D. Lumb,⁴ J.A. Nousek¹ and W.L.W. Sargent⁵

ABSTRACT

We present first results from an X-ray study of the Hubble Deep Field North (HDF-N) and its environs obtained using 166 ks of data collected by the Advanced CCD Imaging Spectrometer (ACIS) on board the *Chandra* X-ray Observatory. This is the deepest X-ray observation ever reported, and in the HDF-N itself we detect six X-ray sources down to a 0.5–8 keV flux limit of $\approx 4 \times 10^{-16}$ erg cm⁻² s⁻¹. Comparing these sources with objects seen in multiwavelength HDF-N studies shows positional coincidences with the extremely red object NICMOS J123651.74 +621221.4, an active galactic nucleus (AGN), three elliptical galaxies, and one nearby spiral galaxy. The X-ray emission from the ellipticals is consistent with that expected from a hot interstellar medium, and the spiral galaxy emission may arise from a ‘super-Eddington’ X-ray binary or ultraluminous supernova remnant. Four of the X-ray sources have been detected at radio wavelengths. We also place X-ray upper limits on AGN candidates found in the HDF-N, and we present the tightest constraints yet on X-ray emission from the SCUBA submillimeter source population. None of the 10 high-significance submillimeter sources reported in the HDF-N and its vicinity is detected with *Chandra* ACIS. These sources appear to be dominated by star formation or have AGN with Compton-thick tori and little circumnuclear X-ray scattering.

Subject headings: diffuse radiation – surveys – cosmology: observations – galaxies: active – X-rays: galaxies – X-rays: general.

¹Department of Astronomy & Astrophysics, 525 Davey Laboratory, Pennsylvania State University, University Park, PA 16802

²Massachusetts Institute of Technology, Center for Space Research, 70 Vassar Street, Building 37, Cambridge, MA 02139

³Department of Physics, Carnegie Mellon University, Pittsburgh, PA 15213

⁴Astrophysics Division, ESTEC, Keplerlaan 1, 2200 AG Noordwijk, The Netherlands

⁵Palomar Observatory, California Institute of Technology, Pasadena, CA 91125

1. Introduction

The Hubble Deep Field North (HDF-N; Williams et al. 1996, hereafter W96) provides an unprecedented view of the distant Universe, and the incredible amount of work focused on this patch of sky has led to fundamental insights about the formation and evolution of galaxies. Intense follow-up studies have been performed at a variety of wavelengths including the radio, submillimeter, far-infrared, near-infrared, and optical bands; these investigations have discovered a fascinating array of cosmic objects. Notably lacking until now, however, is a deep X-ray survey of this area.⁶ X-ray surveys provide the most direct and unbiased probe of massive black hole accretion activity throughout the Universe. This is particularly true in the hard X-ray band above 2 keV where most of the energy density of the extragalactic X-ray background (XRB) resides. In addition, X-ray surveys allow studies of starburst galaxies, elliptical galaxies, clusters and groups of galaxies, and other objects. Early observations with the *Chandra* X-ray Observatory (hereafter *Chandra*; Weisskopf, O’Dell & van Speybroeck 1996) have resolved much ($\gtrsim 60$ –75%) of the 2–8 keV XRB into point sources (Brandt et al. 2000; Mushotzky et al. 2000); an even higher fraction ($\gtrsim 70$ –80%) of the 0.5–2 keV X-ray background had already been resolved by *ROSAT* (e.g., Hasinger et al. 1998). The key goals now remaining are to resolve the rest of the XRB and to understand in detail the nature and evolution of the sources creating it.

In this letter, we present first results from a deep X-ray survey of the HDF-N area using the *Chandra* Advanced CCD Imaging Spectrometer (ACIS; G.P. Garmire et al. 2000, in preparation). We focus on X-ray sources in the HDF-N itself and in its immediate vicinity where substantial follow-up work has already been performed. The Galactic column density along this line of sight is $(1.6 \pm 0.4) \times 10^{20} \text{ cm}^{-2}$ (Stark et al. 1992), and $H_0 = 70 \text{ km s}^{-1} \text{ Mpc}^{-1}$ and $q_0 = 0.5$ are adopted.

2. Chandra ACIS Observations and Data Analysis

The field containing the HDF-N was observed with the *Chandra* ACIS for a total exposure time of 166 ks in three segments on 1999 November 13 (50 ks), 1999 November 14 (58 ks), and 1999 November 21 (58 ks). The HDF-N was placed near the aim point for the ACIS-I array on CCD I3 during all three observations. The full ACIS-I field of view is $16' \times 16'$, and the on-axis image quality is $\approx 0.5''$ FWHM. The observations were corrected for the radiation damage the CCDs suffered during the first few weeks of the mission (Prigozhin et al. 2000; Hill et al. 2000) following the procedure of Townsley et al. (2000), which corrects simultaneously for both position-dependent gain shifts and event grade changes. The three exposures were then co-added after cross-registration using bright sources near the optical axis; we believe cross-registration to

⁶The only previous pointed X-ray observation of the HDF-N was a 21 ks exposure made with the *ROSAT* High Resolution Imager (HRI). No X-ray sources in the HDF-N were detected due to the limited sensitivity of this observation, and to our knowledge the *ROSAT* results have never been published.

be accurate to within $0.3''$. Absolute X-ray source positions are accurate to within $1''$ (see §3.1).

We created images from 0.5–8.0 keV (full band), 0.5–2.0 keV (soft band) and 2–8 keV (hard band) for further study, and we use *ASCA* event grades 0, 2, 3, 4 and 6 in all analyses. We searched these images with the WAVDETECT software (Dobrzycki et al. 1999; Freeman et al. 2000) using the same methods and safety checks as Brandt et al. (2000). We have used a probability threshold of 1×10^{-7} , and light curve analyses verify that none of the X-ray sources discussed below is affected by a ‘flaring pixel’ problem (*Chandra* X-ray Center, private communication). All of the sources below are consistent with being pointlike, although the constraints are not tight in most cases due to limited numbers of photons. Even with a 166 ks observation the data are far from being background limited (the full-band background is 0.037 count pixel $^{-1}$), and within $\approx 3'$ of the aim point the detection limit with our selection criteria is ≈ 7 photons in the full, soft and hard bands. For a power-law model with photon index $\Gamma = 2$ and the Galactic column density, this corresponds to a soft (hard) observed flux detection limit of 2.3×10^{-16} erg cm $^{-2}$ s $^{-1}$ (8.8×10^{-16} erg cm $^{-2}$ s $^{-1}$). For the cosmology of §1, at $z = 1$ the corresponding rest-frame luminosity limits are $L_{1-4 \text{ keV}} = 7.3 \times 10^{41}$ erg s $^{-1}$ ($L_{4-16 \text{ keV}} = 2.6 \times 10^{42}$ erg s $^{-1}$); even fairly low-luminosity Seyfert galaxies should be detected at this redshift. For an open Universe with $q_0 = 0.1$, these limits become $L_{1-4 \text{ keV}} = 1.0 \times 10^{42}$ erg s $^{-1}$ ($L_{4-16 \text{ keV}} = 3.7 \times 10^{42}$ erg s $^{-1}$).

3. Results for Sources in and near the HDF-N

3.1. The X-ray Sources in the HDF-N

We have detected six full-band X-ray sources in the HDF-N (see Table 1 and Figure 1). This number of detections is consistent with plausible extrapolations of the number counts.

Four of the X-ray detections are positionally coincident (to within $0.8''$) with 8.5 GHz sources from Richards et al. (1998, hereafter R98), giving us confidence in these matches and, more generally, in the X-ray positions. **CXOHDFN J123646.4+621404** ($z = 0.960$) is a red spiral galaxy oriented nearly face-on that hosts an active galactic nucleus (AGN; Phillips et al. 1997). Variable radio and optical emission have been detected (R98; Sarajedini et al. 2000). **CXOHDFN J123651.8+621220** is spatially coincident with the remarkable source NICMOS J123651.74+621221.4, the second reddest object in the NICMOS survey of Dickinson et al. (2000). This source is also an 8.5 GHz emitter, and it may have $15 \mu\text{m}$ and 1.3 mm emission as well (R98; Aussel et al. 1999; Downes et al. 1999). While its continuum is very red, it is detected in B_{450} , V_{606} and I_{814} and is thus unlikely to be an extremely high redshift object; photometric redshift estimates indicate $z = 2.6$ – 2.7 , but these have significant uncertainty due to possible reddening by dust (M. Dickinson, private communication). CXOHDFN J123651.8+621220 has the largest hard-band to soft-band count ratio (hereafter ‘band ratio’) of any X-ray source in the HDF-N (see Table 1). Provided the underlying X-ray continuum shape is typical for an AGN with $\Gamma = 1.7$ – 2.1 , the large band ratio suggests substantial internal absorption by a column density $N_{\text{H}} \gtrsim 10^{23}$ cm $^{-2}$. If the

photometric redshift is correct the implied X-ray luminosity is $\gtrsim 10^{44}$ erg s $^{-1}$, and this source would be a good candidate for a type 2 Quasi-Stellar Object.

CXOHDFN J123655.5+621310 ($z = 0.968$) and **CXOHDFN J123657.0+621301** ($z = 0.474$) are both ellipticals with radio emission. The rather flat radio spectrum ($\alpha_r < 0.3$) of the first may suggest AGN activity, although the X-ray luminosity for this object is not unusually high given the large B -band luminosity [$\log(L_B) = 44.52$; compare with Figure 1 of Eskridge, Fabbiano & Kim 1995]. This source has also been detected in the Hogg et al. (2000) survey of the HDF-N at 3.2 μm . The second source has a steep radio spectrum ($\alpha_r = 1.0 \pm 0.3$) as well as a possible ISO detection, and its X-ray luminosity is consistent with that expected from hot gas in an elliptical. Neither of these ellipticals is detected in the hard band, although we cannot rule out the presence of hard power-law emission with luminosity comparable to that seen in some nearby ellipticals (Allen, Di Matteo & Fabian 2000).

The two X-ray sources that are not positionally coincident with radio sources are coincident with fairly bright W96 sources. **CXOHDFN J123641.9+621131** appears to be matched with a bright ($V_{606} = 20.0$) foreground spiral galaxy at $z = 0.089$ lying near the edge of the HDF-N. Somewhat surprisingly, however, the X-ray source position is not consistent with the nucleus of this galaxy. It may be coincident with a bright spot seen clearly in the U_{300} image of W96. If the identification with the galaxy is correct, the X-ray source is ~ 3.5 kpc from the nucleus and its 0.5–8 keV luminosity is 7.2×10^{39} erg s $^{-1}$, low enough that this source might plausibly be an off-nuclear ‘super Eddington’ X-ray binary or ultraluminous supernova remnant (e.g., Fabbiano 1998). The galaxy may also have some 8.5 GHz emission, although this emission is not positionally consistent with the X-ray source (see Table 5 of R98). **CXOHDFN J123648.1+621309** ($z = 0.476$) is another elliptical that has been detected at 3.2 μm by Hogg et al. (2000); its X-ray luminosity is consistent with hot gas emission.

3.2. Active Galactic Nucleus Candidates in the HDF-N

X-ray emission is a universal property of AGN. Several surveys for AGN in the HDF-N itself have been performed, and we have searched for X-ray emission from the resulting AGN candidates of Jarvis & MacAlpine (1998), Conti et al. (1999) and Sarajedini et al. (2000). Aside from CXOHDFN J123646.4+621404, the $z = 0.960$ AGN discussed above, we do not detect any of these candidates, and we place X-ray upper limits as discussed at the end of §2. The physical implications of these upper limits vary depending upon the properties (e.g., optical magnitudes and redshifts) of the individual candidates; given the typical range of X-ray to optical flux for type 1 AGN (e.g., Figure 2 of Schmidt et al. 1998), we should have detected most type 1 AGN to $V \approx 23$ and might plausibly have detected some to $V \approx 27$. We also do not formally detect the $z = 1.013$ strong FR I radio source J123644+621133 (R98), although there is a hint of an X-ray photon excess at its position. Among radio-loud AGN, however, FR I sources are the least X-ray luminous, and a rest-frame X-ray luminosity just below our 2–10 keV upper limit of $\approx 2.2 \times 10^{42}$ erg s $^{-1}$ would still

make this source consistent with the 2–10 keV X-ray luminosities of other FR I sources (compare with Table 3 of Sambruna, Eracleous & Mushotzky 1999).

3.3. Submillimeter Sources in the HDF-N and its Vicinity

Deep submillimeter surveys have revealed a population of luminous, dusty, star-forming galaxies at moderate to high redshift that make an important contribution to the energy output of the Universe (e.g., Hughes et al. 1998, hereafter H98). However, it has been difficult to determine the relative contributions that AGN and star formation make to powering these objects (e.g., Almaini, Lawrence & Boyle 1999). X-ray observations may clearly discriminate between these possibilities.

H98 have presented 5 submillimeter sources in the HDF-N, and Barger et al. (2000, hereafter B00) have presented an additional 5 sources in the vicinity of the HDF-N (here we consider submillimeter sources detected by B00 at $\geq 3\sigma$). All 10 of these sources are in the ACIS field, but we do not detect any of them. Two of these sources may show X-ray photon excesses near their positions, but further observations are needed before source detections can be claimed. We have used the *Chandra* data to place constraints on the primary energy generation mechanism for these 10 sources. We follow the general method described by Fabian et al. (2000, hereafter F00), computing submillimeter (850 μm) to X-ray (2 keV) spectral indices (α_{sx} ⁷) and comparing these with α_{sx} values for local objects (see Table 2 and Figure 2). Because our *Chandra* observation is 8–18 times longer than those used by F00, we are able to place tight α_{sx} constraints on a substantially larger number of submillimeter sources.

One straightforward interpretation of Figure 2 is that star formation is the primary energy source for these 10 submillimeter sources. Black hole accretion could only dominate the energy production if it is either (1) intrinsically X-ray weak or (2) obscured by Compton-thick material along the line of sight and there is little electron scattering by a ‘mirror’ in the nuclear environment. These are the tightest X-ray constraints yet on the submillimeter source population, and the first to apply to enough sources to reasonably represent the population. X-ray background synthesis models suggest that ≈ 10 –20% of the submillimeter sources could be powered by AGN (Almaini et al. 1999), and optical spectroscopy finds indications of AGN activity in at least $\approx 20\%$ of submillimeter sources (Barger et al. 1999). Our 0/10 rate of X-ray detection is uncomfortably small, although it is still statistically consistent with these values at the $\sim 15\%$ level. Although the redshifts used in Figure 2 have significant uncertainties (see H98 and B00), our basic results are not very sensitive to redshift.

If we consider less-significant B00 submillimeter sources in the 2.5–3 σ range, there are two additional 2.8 σ submillimeter sources: 123616.2+621513 (5.4 mJy, z unknown) and 123629.1+621046 (6.1 mJy, $z = 1.013$). Both of these are positionally coincident with *Chandra* sources: CXO-

⁷Note that the ‘s’ in α_{sx} stands for ‘submillimeter’ rather than ‘soft X-ray.’

HDFN J123616.1+621513 (13.5 full-band counts) and CXOHDFN J123629.1+621046 (23.6 full-band counts). The soft-band (hard-band) α_{sx} values for these two sources are > 1.30 ($= 1.22$) and $= 1.31$ (> 1.32), respectively. These sources probably have some AGN activity, although such activity must be obscured or weak.

Additional *Chandra* observations during Cycles 1 and 2 will allow an even deeper (by a factor of 3–6) X-ray survey of this area. Subsequent papers will discuss the X-ray sources detected in the full ACIS field of view and optical follow-up studies.

We thank A. Barger, M. Dickinson, M. Eracleous, A. Fabian, D. Hogg, K. Iwasawa, C. Liu, E. Richards, C. Steidel and R. Williams for helpful discussions and kindly providing data. We thank all the members of the *Chandra* team for their enormous efforts. We gratefully acknowledge the financial support of NASA grant NAS 8-38252 (GPG, PI), NASA GSRP grant NGT5-50247 (AEH), NASA LTSA grant NAG5-8107 and the Alfred P. Sloan Foundation (WNB), and NSF grant AST99-00703 (DPS).

REFERENCES

- Allen, S.W., Di Matteo, T. & Fabian, A.C. 2000, MNRAS, 311, 493
- Almaini, O., Lawrence, A. & Boyle, B.J. 1999, MNRAS, 305, L59
- Aussel, H., Cesarsky, C.J., Elbaz, D. & Starck, J.L. 1999, A&A, 342, 313
- Barger, A.J., Cowie, L.L., Smail, I., Ivison, R.J., Blain, A.W. & Kneib, J.-P. 1999, AJ, 117, 2656
- Barger, A.J., Cowie, L.L. & Richards, E.A. 2000, AJ, in press (B00; astro-ph/0001096)
- Brandt W.N., et al. 2000, AJ, in press (astro-ph/0002121)
- Cohen, J.G., Cowie, L.L., Hogg, D.W., Songaila, A., Blandford, R., Hu, E.M. & Shopbell, P. 1996, ApJ, 471, L5
- Conti, A., Kennefick, J.D., Martini, P. & Osmer, P.S. 1999, AJ, 117, 645
- Dickinson, M., et al. 2000, ApJ, 531, 624
- Dobrzycki, A., Ebeling, H., Glotfelty, K., Freeman, P., Damiani, F., Elvis, M. & Calderwood, T. 1999, *Chandra* Detect 1.0 User Guide. *Chandra* X-ray Center, Cambridge
- Ebeling, H., White, D.A. & Rangarajan, F.V.N. 2000, MNRAS, submitted
- Eskridge, P.B., Fabbiano, G. & Kim, D.-W. 1995, ApJS, 97, 141
- Fabbiano, G. 1998, The Hot Universe: Proceedings of IAU Symposium 188, ed. Koyama, K., Kitamoto, S. & Itoh, M. (Kluwer, Dordrecht), p. 93
- Fabian, A.C., et al. 2000, MNRAS, submitted (F00; astro-ph/0002322)
- Freeman, P.E., Kashyap, V., Rosner, R. & Lamb, D.Q. 2000, ApJ, submitted

- Hasinger, G., Burg, R., Giacconi, R., Schmidt, M., Trümper, J. & Zamorani, G. 1998, *A&A*, 329, 482
- Hill, J.E., Lewis, K.T., Foster, R.F., Bautz, M., Brown, S.K., Roming, P.W.A., Hornschemeier, A.E., Burrows, D.N. & Garmire, G.P. 2000, *Proc. SPIE*, in press
- Hogg, D.W., Neugebauer, G., Cohen, J.G., Dickinson, M., Djorgovski, S.G., Matthews, K. & Soifer, B.T. 2000, *AJ*, in press (astro-ph/9910478)
- Hughes, D.H., et al. 1998, *Nature*, 394, 241 (H98)
- Jarvis, R.M. & MacAlpine, G.M. 1998, *AJ*, 116, 2624
- Kraft, R.P., Burrows, D.N. & Nousek, J.A. 1991, *ApJ*, 374, 344
- Lyons, L. 1991, *Data Analysis for Physical Science Students*. Cambridge University Press, Cambridge
- Mushotzky, R.F., Cowie, L.L., Barger, A.J. & Arnaud, K.A. 2000, *Nature*, in press (astro-ph/0002313)
- Phillips, A.C., Guzmán, R., Gallego, J., Koo, D.C., Lowenthal, J.D., Vogt, N.P., Faber, S.M., Illingworth, G.D. 1997, *ApJ*, 489, 543
- Prigozhin, G., Kissel, S., Bautz, M., Grant, C., LaMarr, B., Foster, B. & Ricker, G. 2000, *Proc. SPIE*, in press
- Richards, E.A., Kellermann, K.I., Fomalont, E.B., Windhorst, R.A. & Partridge, R.B. 1998, *AJ*, 116, 1039 (R98)
- Sambruna, R.M., Eracleous, M., & Mushotzky, R.F. 1999, *ApJ*, 526, 60
- Sarajedini, V.L., Gilliland, R.L. & Phillips, M.M. 2000, *AJ*, in press
- Schmidt, M., Hasinger, G., Gunn, J., Schneider, D., Burg, R., Giacconi, R., Lehmann, I., MacKenty, J., Trümper, J. & Zamorani, G. 1998, *A&A*, 329, 495
- Stark, A.A., Gammie, C.F., Wilson, R.W., Bally, J., Linke, R.A., Heiles, C. & Hurwitz, M. 1992, *ApJS*, 79, 77
- Townsley, L.K., Broos, P.S., Garmire, G.P. & Nousek, J.A. 2000, *ApJ*, in press (astro-ph/0004048)
- Weisskopf, M.C., O’Dell, S.L. & van Speybroeck, L. 1996, *Proc. SPIE*, 2805, 2
- Williams, R.E., et al. 1996, *AJ*, 112, 1335 (W96)

Table 1. Properties of ACIS HDF-N Sources

CXOHDFN Name (J2000)	Off axis Angle (')	0.5–8.0 keV Counts ^a	Band Ratio ^b	$F_{0.5-8}$ (erg cm ⁻² s ⁻¹) ^c	$L_{0.5-8}$ (erg s ⁻¹) ^d	W96 Name	CXO/W96 Offset (") ^e	Redshift ^f	V_{606}^g	Descriptive Notes ^h
123641.9+621131	2.65	7.4 ± 2.8	$< 1.92^{+2.10}_{-0.66}$	3.9×10^{-16}	7.2×10^{39}	4-976	1.92	0.089 ¹	20.0	Spiral
123646.4+621404	2.03	220.4 ± 15.0	$1.26^{+0.18}_{-0.16}$	1.2×10^{-14}	3.3×10^{43}	2-251	0.74	0.960 ²	22.5	AGN (R)
123648.1+621309	1.51	8.3 ± 3.0	$< 1.02^{+0.67}_{-0.29}$	4.4×10^{-16}	2.7×10^{41}	2-121	0.62	0.476 ³	21.4	Elliptical
123651.8+621220	1.23	29.9 ± 5.6	$3.30^{+2.22}_{-1.16}$	3.1×10^{-15}	1.7×10^{44}	—	0.76	2.6–2.7 ⁴	26.7	NICMOS (R)
123655.5+621310	0.68	25.0 ± 5.1	$< 0.36^{+0.11}_{-0.07}$	1.3×10^{-15}	3.9×10^{42}	3-180	0.73	0.968 ⁵	23.2	Elliptical (R)
123657.0+621301	0.48	10.2 ± 3.3	$< 1.16^{+0.86}_{-0.35}$	5.4×10^{-16}	3.2×10^{41}	3-355	0.53	0.474 ⁶	24.4	Elliptical (R)

^aSource counts and errors are as computed by WAVDETECT (see Freeman et al. 2000 for details).

^bDefined as the ratio of counts between the 2–8 keV and 0.5–2 keV bands. Errors for this quantity are calculated following the ‘numerical method’ described in §1.7.3 of Lyons (1991).

^cFluxes in this column are for the observed frame and are not corrected for Galactic absorption. For all sources other than 123651.8+621220, fluxes have been computed adopting a power-law model with photon index $\Gamma = 2$ and the Galactic column density. For 123651.8+621220 we also include a column density of 10^{23} cm⁻² at $z = 2.6$ (see §3.1).

^dLuminosities are for the rest frame and are corrected for Galactic absorption. We again adopt a power-law model with $\Gamma = 2$. For 123651.8+621220 we also correct for the probable intrinsic absorption (see note c), and we adopt the photometric redshift estimate of $z = 2.6$ for lack of a spectroscopic redshift (see §3.1). The 2–8 keV luminosity for 123651.8+621220 is 9.3×10^{43} erg s⁻¹, and this quantity is relatively insensitive to corrections for internal absorption.

^eOffset between the *Chandra* source and the proposed W96 identification. For 123651.8+621220 we quote the offset from NICMOS J123651.74+621221.4.

^fRedshift references are indicated by numerical superscripts as follows: (1) Cohen et al. (1996), (2) Phillips et al. (1997), (3) Hogg et al. (2000), (4) M. Dickinson, private communication, (5) Hogg et al. (2000), (6) Barger et al. (2000). The redshift for CXOHDFN 123651.8+621220 is photometric and subject to significant uncertainty (see §3.1).

^gAll V_{606} magnitudes other than that for 123651.8+621220 are from W96. The V_{606} magnitude for 123651.8+621220 is from M. Dickinson, private communication.

^hSources with ‘(R)’ are 8.4 GHz sources from R98.

Table 2. *Chandra* Constraints on 850 μm Sources

Source Name	S_{850} (mJy) ^a	$F_{0.5-2}/F_{2-8}^b$	0.5–2 keV α_{sx} / 2–8 keV α_{sx}^c
HDF 850.1	7.0	< 1.5 / < 8.3	> 1.37 / > 1.26
HDF 850.2	3.8	< 2.1 / < 5.8	> 1.31 / > 1.24
HDF 850.3	3.0	< 1.5 / < 8.3	> 1.32 / > 1.20
HDF 850.4	2.3	< 2.1 / < 10.5	> 1.28 / > 1.17
HDF 850.5	2.1	< 1.5 / < 5.8	> 1.29 / > 1.20
123618.3+621551	7.8	< 1.6 / < 9.0	> 1.38 / > 1.26
123621.3+621708	7.5	< 2.3 / < 6.5	> 1.36 / > 1.28
123622.7+621630	7.1	< 2.2 / < 9.0	> 1.35 / > 1.26
123646.1+621449	10.7	< 2.7 / < 13.2	> 1.37 / > 1.26
123700.3+620910	11.9	< 1.6 / < 9.0	> 1.41 / > 1.29

^a850 μm flux density.

^bFluxes in this column are in units of 10^{-16} erg cm^{-2} s^{-1} . They are for the observed frame and are not corrected for Galactic absorption. They have been computed adopting a power-law model with photon index $\Gamma = 2$ and the Galactic column density. Upper limits are calculated using the Bayesian method of Kraft, Burrows & Nousek (1991) for 99% confidence; the uniform prior used by these authors results in fairly conservative upper limits, and other reasonable choices of priors do not materially change our scientific results.

^cThe ‘0.5–2 keV α_{sx} ’ uses a 2 keV flux density derived by converting the observed 0.5–2 keV counts into a flux. The ‘2–8 keV α_{sx} ’ is derived in a similar manner using the 2–8 keV counts. Spectral models are as per note b, and the flux densities used are for the observed frame.

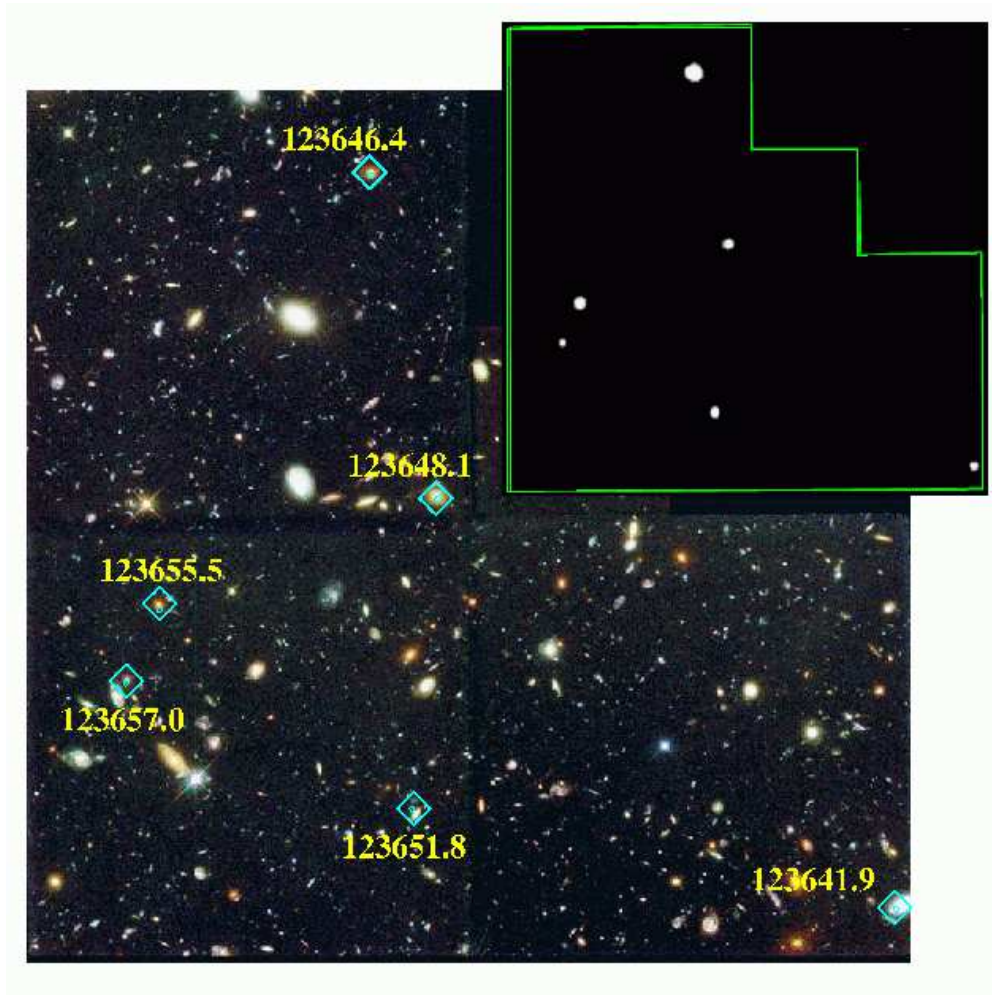


Fig. 1.— The main image shows the *Chandra* sources detected in the HDF-N overlaid on the W96 optical image. *Chandra* sources are labeled by the right ascension parts of their CXO names (see Table 1). The small ellipses inside the diamonds have sizes that approximately match our statistical positional uncertainties (the diamonds are drawn only to help the reader locate the ellipses). The smaller image to the upper right shows the *Chandra* image after adaptive smoothing using the code of Ebeling, White & Rangarajan (2000). The smoothing has been performed at the 2.5σ level.

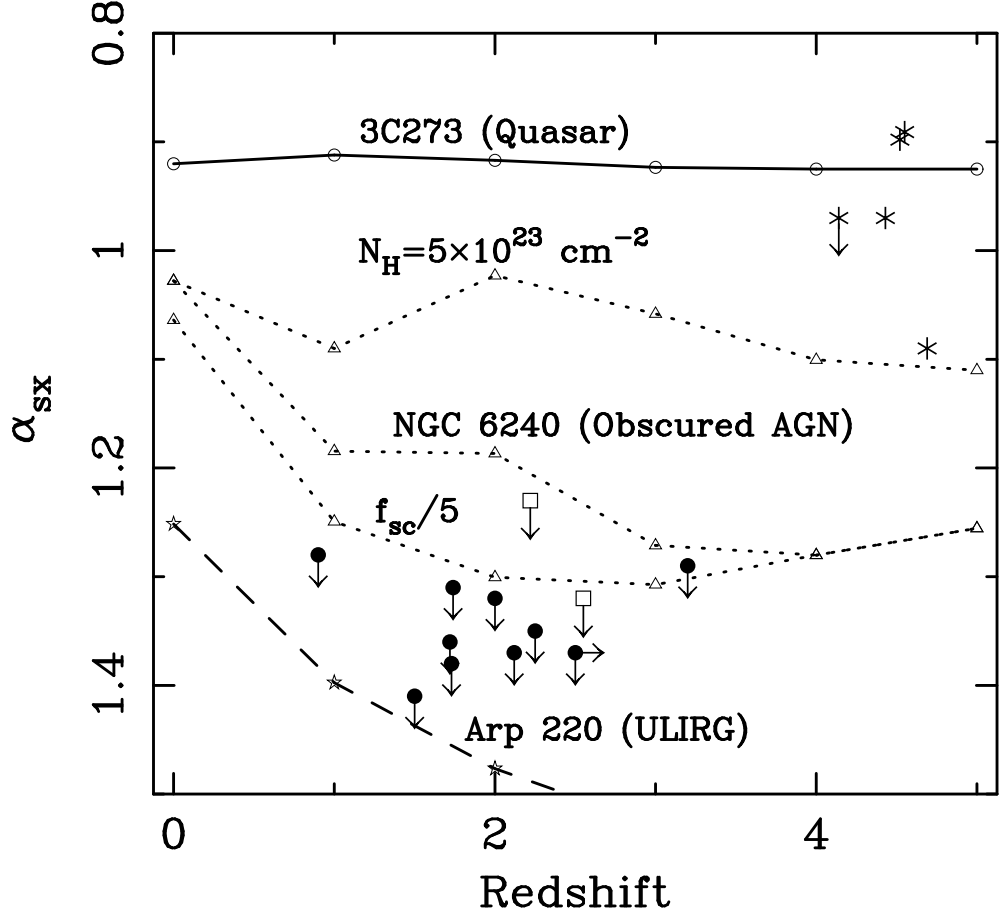


Fig. 2.— Submillimeter to X-ray spectral index (α_{sx}) plotted against redshift (adapted from F00). Shown are the quasar 3C273 (solid curve), the ultraluminous obscured ($N_{\text{H}} \approx 2 \times 10^{24} \text{ cm}^{-2}$) AGN NGC 6240 (dotted curves), the ultraluminous infrared galaxy (ULIRG) Arp 220 (dashed curve), five $z > 4$ quasars (asterisks), two submillimeter sources from F00 (open squares), and the 10 submillimeter sources from the HDF-N and its vicinity (solid dots; these are our 0.5–2 keV α_{sx} values). For NGC 6240, the effects of decreasing its column density to $5 \times 10^{23} \text{ cm}^{-2}$ and its scattered X-ray fraction by a factor of 5 are also shown. For the HDF-N area submillimeter sources we have calculated millimetric redshifts following B00 when possible; see B00 for a discussion of the errors associated with these. For HDF 850.3, HDF 850.4 and HDF 850.5 we have used the redshift estimates from Table 2 of H98.